ELSEVIER

Composites: Part B 32 (2001) 599–607

composites
Part B: engineering

www.elsevier.com/locate/compositesb

Effects of low temperature on the dynamic moduli of thick composite beams with absorbed moisture

K.H. Ip[a,*], P.K. Dutta[b], D. Hui[c]

[a]*Department of Mechanical Engineering, The Hong Kong Polytechnic University, c/o Prof. P.C. Tse, Hung Hom, Kowloon, Hong Kong, People's Republic of China*
[b]*US Army Cold Regions Research and Engineering Laboratory, Hanover, NH 03755, USA*
[c]*Department of Mechanical Engineering, University of New Orleans, New Orleans, LA 70148, USA*

Received 6 January 2001; accepted 28 May 2001

Abstract

The present investigation concentrates on the influence of low temperature and moisture on the dynamic moduli of thick S2-glass composite beams. By supporting the beam sample in a free–free configuration, its natural frequencies were obtained through impact testing. Frequency dependence on the hydrothermal conditions was disclosed by testing the sample at different temperatures and with different moisture contents. Based on the frequency measurements, a method was developed to predict the longitudinal Young's modulus and the transverse shear modulus of the sample. The process involves iterative tuning of the moduli of a Timoshenko beam model via a stable characterization scheme. Numerical sensitivity study shows that the moduli thus determined are insensitive to measurement errors rendering the method a possible supplement for conventional static tests. Both frequencies and moduli of the beam sample were found to exhibit an increasing trend with reducing temperature. Besides, freezing of the absorbed moisture enlarged the longitudinal Young's modulus of the material in a significant manner.

Keywords: Dynamic moduli

1. Introduction

Advanced fiber-reinforced composites have gained wide use in engineering structures. The advantages of these materials are derived from their high strength, stiffness and damping together with low specific weight. More important, they offer the potential of reducing costs in construction, operation and development while improving structural reliability and enhancing safety. Examples of their use can be found in the load bearing components of aerospace vehicles, military and civilian aircraft. In these applications, composites are usually exposed to severe hydrothermal conditions. It has been recognized that both temperature and absorbed atmospheric moisture can have significant effects on the mechanical properties of composite materials. A clear knowledge of these effects is thus vital before composites can be put to optimal use.

In recent decades, much attention has been given to the establishment of reliable tests on the hygrothermal behavior of fiber-reinforced composites. Most of them focused on the static response of fiber-reinforced composites. Hertz [1] performed a wide variety of experiments on the high temperature performance of commercial epoxy resins and composites under wet-aged conditions. Moisture was found to be an important factor causing the loss in the high temperature flexural moduli of samples. The tests also yielded valuable data for the study of moisture diffusion in both resins and composites. Allred [2,3] carried out a similar investigation into the moisture effects on the flexural moduli and strengths of Kevlar/epoxy laminates over a large temperature range from −55 to 150°C. Introduction of moisture into the specimens leads to a progressive depression of their stiffnesses as temperature rises. In addition, a slight enhancement of modulus at low temperatures was reported. Flexural test data of the Kevlar/epoxy specimens also indicated that hygrothermal effects altered the strength of composites. It was found that in the high temperature region, wet-aged conditions lead to a substantial degradation of strength. Yet a reverse behavior was noticed at low temperatures in which failure was inhabited by the absorbed moisture. Apart from static tests, experiments on the temperature and moisture effects on the dynamic characteristics of fiber-reinforced composites were also conducted. The tests reveal that dynamic moduli

* Corresponding author.

1359-8368/01/$ - see front matter
PII: S1359-8368(01)00037-3

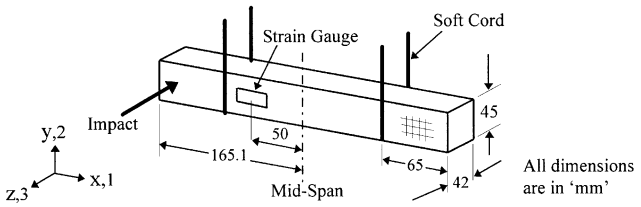

Fig. 1. Configuration of the specimen in vibration test.

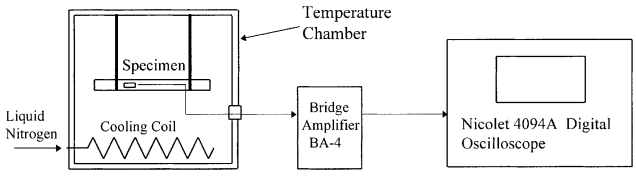

Fig. 2. Schematic diagram of the setup for vibration test.

of composites are more susceptible to temperature variation if the fibers are perpendicular rather than parallel to the stress direction. Like static moduli, dynamic moduli exhibit decreasing trend with increasing temperature. The presence of moisture was found to exaggerate such depression in the high temperature regime. It is suspect that the reduction of matrix glass transition temperature due to moisture is a primary reason causing the above degradation. Similar investigation into the hygrothermal response of chopped fiber composite beams was carried out by Gibson et al. [4]. They found that the dynamic moduli decreased whereas the damping increased at elevated temperatures. A comprehensive review on the hydrothermal effects on both static and dynamic moduli of graphite/epoxy composites was given by Lee and Peppas [5]. This article also summarizes the investigations on various aspects like swelling, plasticizing and microcracking of resins as well as moisture diffusion and residual stresses in composites. Most of the aforementioned studies, however, address to the behavior of composites at elevated temperatures.

Standard method like ASTM Three-Point Bending Test (D790) is available to characterize the flexural moduli of composite beams. Advantages of this method are derived from its simplicity to run and instrument. The test, however, is not recommended for thick-section samples in which transverse shear and transverse normal deformations are significant. The effect is more pronounce in composites, which usually have small transverse shear modulus. Fischer et al. [6] proposed a method for the simultaneous determination of longitudinal Young's moduli and transverse shear moduli of thick beams using three-point bending test. Yet, two major problems still remain. The first one arises from buckling of fibers on the compressive side of the sample, especially for thick samples where large stresses are involved. Fiber buckling causes nonlinearity in the load-deflection curves and hence introduces difficulty into the data reduction process. A feasible solution is to keep the strains of the sample below an acceptably low level during the characterization process. One technique fulfilling such requirement is the vibration test. An increasing popularity of this method is observed in recent decades and relevant standard like ASTM (C1259) has been established. Advantages of vibration test are derived from its repeatability and accuracy along with its simplicity to run and setup. However, conversion of the vibration test data to the dynamic moduli of samples requires an inverse calculation scheme. In this connection, a highly convergent and self-starting inverse calculation scheme is developed in this paper.

2. Low temperature impact test

Impact test was performed on a typical S2-glass woven fabric and polyester resin composite beam. The specimen is 330.2 mm long with a rectangular cross-section of 42×45 mm^2. The equivalent density of the constituting material is 1890 kg/m^3. During the test, the sample was hung in a free–free configuration by soft cords as shown in Fig. 1. x–y–z represents a Cartesian coordinate system whose axes coincide with the principal material directions (1–2–3) of the beam. To monitor the flexural response, a strain gauge was installed to measure the longitudinal strain. The strain gauge was deliberately made offset from the mid-span of the beam in order to monitor straining from both the symmetric and antisymmetric modes of vibration. The whole system was subsequently housed inside a well-insulated temperature chamber for low temperature testing.

To set the sample into free vibration, a transverse impact parallel to the z-axis was given as shown in Fig. 1. Outputs from the strain gauge were amplified by a bridge amplifier and were subsequently recorded by a Nicolet 4094A Digital Oscilloscope. Since it is desired to measure those frequencies up to 5 kHz, the dynamic signal was sampled at 100 μs intervals to avoid aliasing. Pre-triggering of 0.1 s was also activated in order to capture the whole flexural response during the impact. A schematic diagram of the experimental setup is shown in Fig. 2. Discrete Fourier transform was subsequently performed on the captured signal via the Fast Fourier Transform (FFT) algorithm. Such algorithm operates on 2048 captured strain data resulting in a frequency spectrum of 4.88 Hz resolution. Fig. 3(a) and (b) shows a typical time history of the captured strain data and the corresponding frequency spectrum. Notice that the measured strains are very small as they are well below 100 με throughout the test. From the frequency spectrum, two peaks at frequencies f_1 and f_2 are identified, which represent the natural frequencies of the first two flexural modes of the beam in the x–z plane.

The effects of low temperature on the vibration characteristic of the beam sample were revealed by repeating the impact test at different temperatures. It is worth mentioning that the strain gauge needed not be calibrated despite the

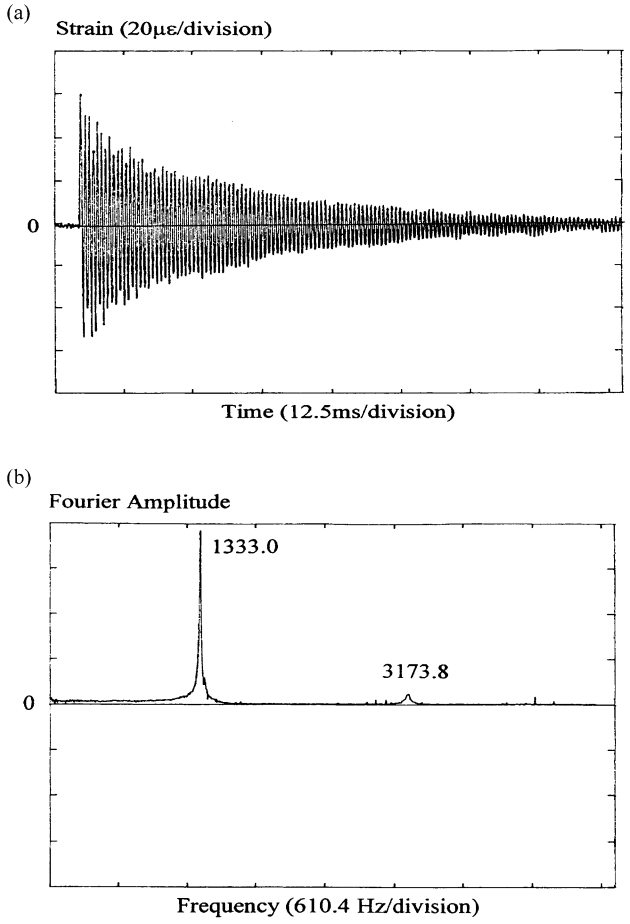

Fig. 3. (a) Typical strain signal captured by the digital oscilloscope; (b) frequency spectrum of (a).

temperature change, as the frequency of straining rather than the actual strain value is required. To provide a low temperature environment for testing, the interior of the temperature chamber was cooled by evaporating liquid nitrogen. A fan was also equipped to distribute the nitrogen gas. Temperature of the specimen itself was monitored by a thermocouple. Three more thermocouples were attached to another similar sample inside the chamber. It took about 20 min for the four thermocouple readings to stabilize to ±1°C from their average. The first two natural frequencies of the specimen were then measured over the temperature range from 24°C (room temperature) down to −80°C. After completing the low temperature tests, the sample was tested again at room temperature. There is no observable change in its frequencies implying that the low temperature vibration test is non-destructive. To study the effects of moisture on its vibration characteristics, the beam sample was soaked with water prior to another set of impact tests. In the soaking test, the beam was immersed in a distilled water bath at 22.3°C. It took about 117 h of soaking to achieve saturation. For comparison purpose, natural frequencies of the same specimen after oven-drying were also measured. The drying test was performed by putting the specimen inside an oven at 90°C. The sample was found to be over-dried after 120 h. Making use of the results from the soaking and drying tests, weight percents of water present in the sample before and after soaking are found to be 0.46 and 0.93%, respectively.

Table 1
Frequencies of S2-glass composite beam measured at different temperatures

Temperature (°C)	Resonant frequency (Hz)	
	f_1	f_2
24.00	1333.0	3173.8
17.00	1337.9	3173.8
9.00	1337.9	3178.7
0.25	1342.8	3188.5
−8.00	1396.5	3315.4
−16.25	1416.0	3359.4
−23.25	1425.8	3388.7
−30.75	1435.5	3427.7
−39.50	1445.3	3447.3
−45.50	1445.3	3457.0
−52.50	1450.2	3481.4
−60.25	1450.2	3491.2
−67.50	1455.1	3501.0
−74.50	1460.0	3515.6
−81.25	1464.8	3530.3

3. Experimental results

The first two natural frequencies f_1 and f_2 of the original sample, and that after the soaking and drying tests, are tabulated against temperature in Tables 1–3. Frequency variations due to temperature change are then plotted in Figs. 4–6. Regarding each of the frequency pairs in Tables 1–3 as the target response, both E_{11} and G_{13} in an analytical beam model are adjusted in order to converge the theoretical frequencies and the measurements. After this adjustment procedure, the resulting moduli are considered the true

Table 2
Frequencies of S2-glass composite beam measured after the soaking test

Temperature (°C)	Resonant frequency (Hz)	
	f_1	f_2
25.32	1328.1	3168.9
19.47	1337.9	3183.6
7.79	1347.7	3198.2
0.00	1347.7	3208.0
−7.79	1425.8	3378.9
−11.68	1430.7	3413.1
−15.57	1435.5	3432.6
−19.47	1440.4	3452.1
−23.37	1445.3	3461.9
−33.11	1455.1	3501.0
−44.79	1469.7	3535.2
−52.57	1474.6	3549.8
−60.37	1484.4	3574.2
−71.08	1489.3	3598.6
−79.84	1494.1	3608.4

Table 3
Frequencies of S2-glass composite beam measured after the drying test

Temperature (°C)	Resonant frequency (Hz)	
	f_1	f_2
25.32	1328.1	3144.5
18.50	1328.1	3144.5
10.71	1333.0	3159.2
5.84	1333.0	3168.9
0.00	1333.0	3173.8
−7.79	1337.9	3183.6
−12.66	1337.9	3193.4
−17.53	1342.8	3203.1
−22.39	1342.8	3208.0
−28.24	1342.8	3212.9
−35.05	1347.7	3217.8
−42.84	1347.7	3222.7
−50.63	1352.5	3232.4
−59.39	1357.4	3247.1
−71.08	1362.3	3261.7
−80.82	1367.2	3276.4

material properties of the sample. Since the cross-sectional dimensions of the sample are not small as compared to its length, it is considered as a thick beam. Its flexural response is therefore susceptible to both rotary inertia and transverse shear deformation. Consequently, an accurate modeling requires the thick beam theory known as the Timoshenko beam theory; see Ref. [7].

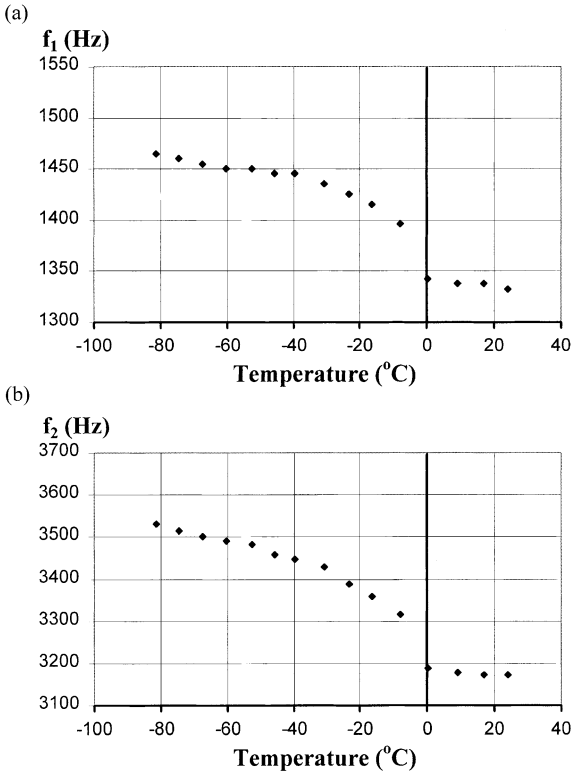

Fig. 4. Effects of low temperature on frequencies (a) f_1 and (b) f_2 of S2-glass composite beam.

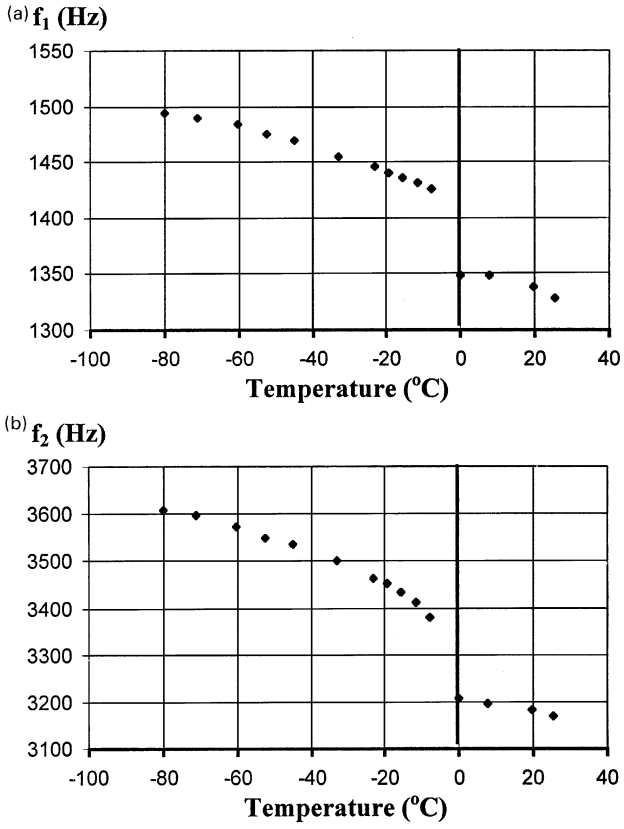

Fig. 5. Effects of low temperature on frequencies (a) f_1 and (b) f_2 of soaked S2-glass composite beam.

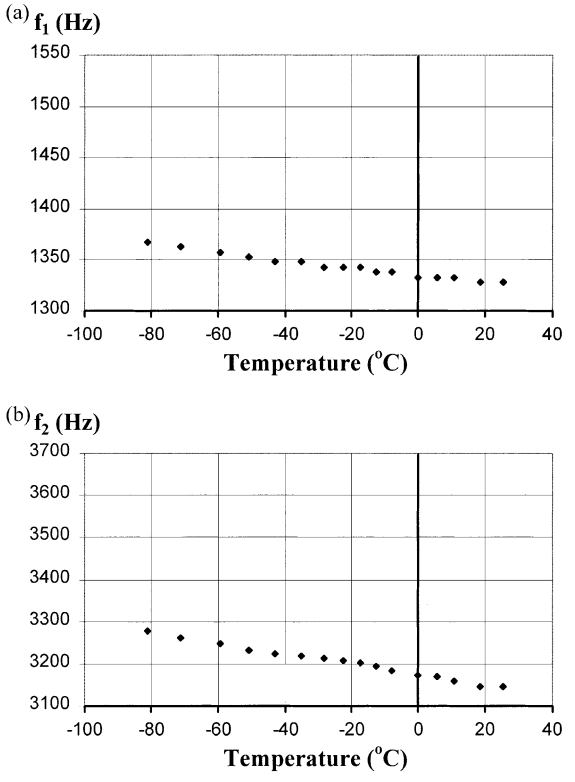

Fig. 6. Effects of low temperature on frequencies (a) f_1 and (b) f_2 of dried S2-glass composite beam.

4. Timoshenko beam theory

The equations of motion for a Timoshenko beam under free flexural vibration in the x–z plane are

$$E_{11}I\frac{\partial^4 w}{\partial x^4} + \rho A\frac{\partial^2 w}{\partial t^2} - \rho I\left(1 + \frac{E_{11}}{kG_{13}}\right)\frac{\partial^4 w}{\partial x^2 \partial t^2} + \frac{\rho^2 I}{kG_{13}}\frac{\partial^4 w}{\partial t^4} = 0 \tag{1a}$$

and

$$E_{11}I\frac{\partial^4 \psi}{\partial x^4} + \rho A\frac{\partial^2 \psi}{\partial t^2} - \rho I\left(1 + \frac{E_{11}}{kG_{13}}\right)\frac{\partial^4 \psi}{\partial x^2 \partial t^2} + \frac{\rho^2 I}{kG_{13}}\frac{\partial^4 \psi}{\partial t^4} = 0 \tag{1b}$$

where w is the transverse deflection of the centerline of the beam, ψ the slope of the centerline due to bending, A the cross-section area of the beam, I the second moment of area about the principal axis normal to the x–z plane, ρ the mass density of the composite material, k is the factor which depends on the shape of the cross section. For beams having a rectangular cross-section, k is assigned a value of 2/3; see Ref. [8]. In accordance with White and Heppler [9], using separation of variables in the form

$$w(x,t) = W(x)\,e^{j\omega t} \qquad \text{and} \qquad \psi(x,t) = \Psi(x)\,e^{j\omega t} \tag{2}$$

$W(x)$ and $\Psi(x)$ are found to be

$$W(x) = C_1\cosh(b\alpha\xi) + C_2\sinh(b\alpha\xi) + C_3\cos(b\beta\xi) + C_4\sin(b\beta\xi) \tag{3a}$$

and

$$\Psi(x) = C_1\left[\frac{b}{L}\left(\frac{\alpha^2 + s^2}{\alpha}\right)\right]\sinh(b\alpha\xi) + C_2\left[\frac{b}{L}\left(\frac{\alpha^2 + s^2}{\alpha}\right)\right]\cosh(b\alpha\xi) - C_3\left[\frac{b}{L}\left(\frac{\beta^2 - s^2}{\beta}\right)\right]\sin(b\beta\xi) + C_4\left[\frac{b}{L}\left(\frac{\beta^2 - s^2}{\beta}\right)\right]\cos(b\beta\xi) \tag{3b}$$

where

$$\xi = \frac{x}{L}, \qquad b^2 = \frac{\rho A L^4 \omega^2}{E_{11}I}, \qquad r^2 = \frac{I}{AL^2},$$

$$s^2 = \frac{E_{11}I}{kAG_{13}L^2}$$

and

$$\begin{pmatrix}\alpha\\ \beta\end{pmatrix} = \frac{1}{\sqrt{2}}\left[\pm(r^2 + s^2) + \sqrt{(r^2 - s^2) + \frac{4}{b^2}}\right]^{1/2}$$

Parameters r and s account for the effects of rotary inertia and transverse shear deformation, respectively. Notice that the angular frequency ω is related to the natural frequency f by

$$\omega = 2\pi f$$

For a free–free beam, the shear force and bending moment should vanish at both ends. Applying such boundary conditions to the general solutions in Eqs. (3a) and (3b) leads to the frequency equation

$$\frac{1}{2}\left[\frac{\alpha}{\beta}\left(\frac{\alpha^2 + s^2}{\beta^2 - s^2}\right) - \frac{\beta}{\alpha}\left(\frac{\beta^2 - s^2}{\alpha^2 + s^2}\right)\right]\sinh(b\alpha)\sin(b\beta) + \cosh(b\alpha)\cos(b\beta) = 1 \tag{4}$$

Notice from this equation that apart from the physical properties of the beam, it relates the angular frequency ω to the longitudinal Young's modulus E_{11} and the transverse shear modulus G_{13}. Care should be taken when exercising this frequency equation if

$$(r^2 + s^2) > \sqrt{(r^2 - s^2) + \frac{4}{b^2}}$$

or, after simplification,

$$\omega^2 > \frac{kG_{13}A}{\rho I} \tag{5}$$

Under this condition, α becomes imaginary and Eq. (4) should take another form corresponding to a 'second frequency spectrum'; see Ref. [10]. Levinso and Cooke [11] have corrected such 'two frequency spectra' viewpoint in an article based on elementary analysis. As far as the present investigation is concerned, all natural modes in the second spectrum have too a high frequency to be encountered.

5. Inverse calculation scheme

An iterative procedure which enables an efficient adjustment of both E_{11} and G_{13} in the Timoshenko beam model are described. For a given sample under a specific environmental condition, an initial guess for E_{11} and its angular frequency ω_2 are first substituted into Eq. (4). Solving the resulting equation will lead to an estimate for G_{13}. Incorporation of this property and the angular frequency ω_1 into the characteristic equation in turn gives a new estimate for E_{11}. This E_{11} value is now fed back as an improved initial guess and the above steps are repeated. The iteration terminates when both E_{11} and G_{13} agree with their prior values by three decimal places. The converged

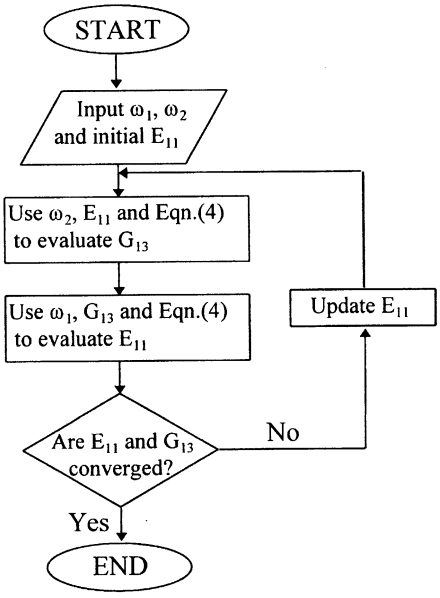

Fig. 7. Flow chart for the inverse calculation scheme.

moduli are then considered as the true material properties of the beam sample. A flow chart summarizing the whole characterization procedure is given in Fig. 7.

6. Iteration results

Recall that the characterization process in Fig. 7 requires an input of two frequency measurements ω_1 and ω_2 along with an initial guess for E_{11}. For unidirectional or woven fabric composites, the initial E_{11} value can be evaluated using the rules of mixtures; see Ref. [12]. Alternatively, an estimate for E_{11} can be obtained using the Bernoulli–Euler beam model; see Ref. [8]. This model neglects both rotary inertia and transverse shear deformation. For a Bernoulli–Euler beam with free–free boundaries, E_{11} is related to the fundamental frequency ω_1 by

$$E_{11} = \frac{\rho A L^4}{I}\left(\frac{\omega_1}{22.4}\right)^2 \tag{6}$$

Table 4
Values for E_{11} and G_{13} of S2-glass composite beam at 24°C during the iterative process

Iteration step	E_{11} (GPa)	G_{13} (GPa)
Initial Guess	21.369	–
1	24.107	9.631
2	25.026	5.792
3	25.298	5.208
4	25.376	5.064
5	25.398	5.025
6	25.404	5.014
7	25.406	5.011
8	25.407	5.010
Converged result	25.407	5.010

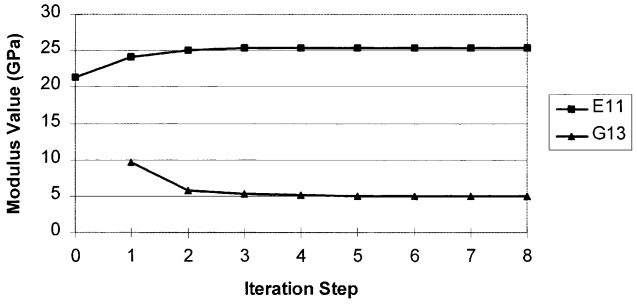

Fig. 8. Convergence graph for E_{11} and G_{13} of S2-glass composite beam at 24°C.

As the fundamental frequency ω_1 of the sample is already measured, E_{11} is readily obtained. Consequently, the inverse calculation process becomes self-starting. Consider the sample at 24°C (room temperature) as an example, its E_{11} and G_{13} values throughout the iterative process are presented in Table 4. The corresponding convergence graph is shown in Fig. 8.

By incorporating the frequency pairs in Tables 1–3 into the inverse calculation scheme, the longitudinal Young's moduli and the transverse shear moduli of the sample at different temperatures are evaluated. These characterized moduli are tabulated in Tables 5–7 and are plotted against temperatures in Figs. 9–11. For the ease of comparison, those graphs associated with the same property are plotted in the same scale. Fast convergence of the inverse calculation is observed in which all the characterization processes terminate within 10 iteration steps.

7. Discussion

It is observed from Figs. 4–6 that frequencies of the S2-glass composite beam exhibit a monotonic increasing trend with decreasing temperature. The apparent stationary

Table 5
Characterized E_{11} and G_{13} values of S2-glass composite material at different temperatures

Temperature (°C)	E_{11} (GPa)	G_{13} (GPa)
24.00	25.407	5.010
17.00	25.698	4.873
9.00	25.654	4.945
0.25	25.859	4.953
−8.00	27.974	5.348
−16.25	28.782	5.463
−23.25	29.125	5.634
−30.75	29.372	5.977
−39.50	29.810	5.993
−45.50	29.719	6.163
−52.50	29.803	6.442
−60.25	29.714	6.636
−67.50	29.933	6.641
−74.50	30.110	6.742
−81.25	30.279	6.853

Table 6
Characterized E_{11} and G_{13} values of S2-glass composite material after the soaking test

Temperature (°C)	E_{11} (GPa)	G_{13} (GPa)
25.32	25.162	5.079
19.47	25.610	5.018
7.79	26.062	4.963
0.00	25.975	5.110
−7.79	29.215	5.483
−11.68	29.203	5.884
−15.57	29.329	6.062
−19.47	29.456	6.246
−23.37	29.674	6.253
−33.11	29.932	6.641
−44.79	30.548	6.753
−52.57	30.724	6.858
−60.37	31.124	6.968
−71.08	31.212	7.289
−79.84	31.436	7.291

frequencies at varying temperature result from the finite resolution of the frequency spectrum. Except for the over-dried sample whose frequency plots are nearly a straight line, frequency jumps at 0°C are observed in the other frequency curves. An immediate conclusion is that material property of the wet-aged sample should also exhibit a similar change at the freezing point.

Figs. 9–11 show the variations of longitudinal Young's modulus E_{11} and transverse shear modulus G_{13} of the composite material at different temperatures and moisture contents. At temperatures between 0 and 24°C, both moduli are insensitive to the absorbed moisture and temperature. Below the freezing point, however, the presence of moisture inside the composite increases the stiffness sensitivity to temperature. Over the entire temperature range from 24 to −80°C, E_{11} and G_{13} of the dried sample show a linearly increasing trend with the cooling run. These moduli are

Table 7
Characterized E_{11} and G_{13} values of S2-glass composite material after the drying test

Temperature (°C)	E_{11} (GPa)	G_{13} (GPa)
25.32	25.378	4.716
18.15	25.378	4.716
10.71	25.537	4.794
5.84	25.450	4.936
0.00	25.407	5.010
−7.79	25.610	5.018
−12.66	25.524	5.171
−17.53	25.727	5.179
−22.39	25.685	5.257
−28.24	25.643	5.338
−35.05	25.888	5.265
−42.84	25.846	5.345
−50.63	26.050	5.352
−59.39	26.212	5.441
−71.08	26.375	5.531
−80.82	26.539	5.623

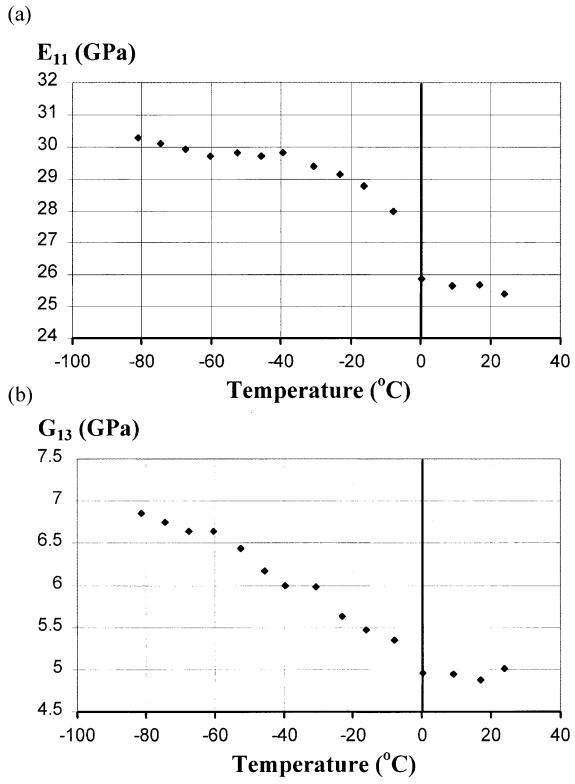

Fig. 9. Effects of low temperature on (a) E_{11} and (b) G_{13} of S2-glass composite beam.

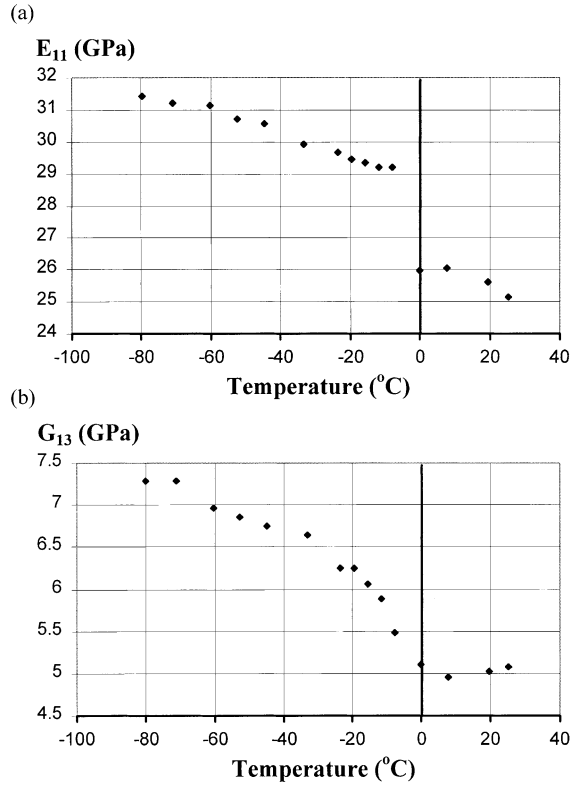

Fig. 10. Effects of low temperature on (a) E_{11} and (b) G_{13} of soaked S2-glass composite beam.

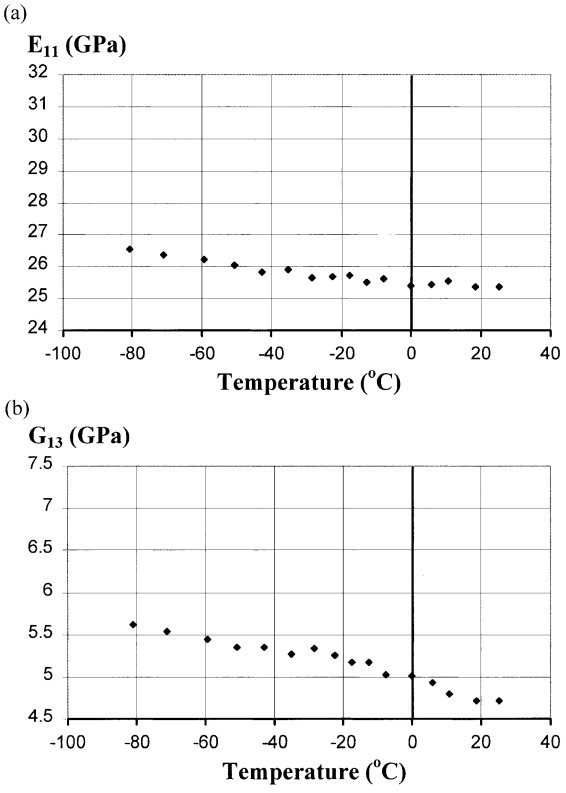

Fig. 11. Effects of low temperature on (a) E_{11} and (b) G_{13} of dried S2-glass composite beam.

enhanced by 4.57 and 19.23%, in respective, from their room temperature values. Such percentages are exaggerated for samples having high moisture contents. As in the saturated beam, these percentages were increased to 24.93 and 43.55% under the most severe conditions. Comparison of these percentages reveals that G_{13}, which is matrix dominant, is more susceptible to temperature variation than E_{11}. Besides, the examination of Figs. 9 and 10 discloses that E_{11} changes significantly at 0°C which explains the frequency jumps in Figs. 4 and 5. No such observation in the dried sample suggests that the property change is attributed to freezing of the absorbed moisture. The freezing process begins with freezing of water pockets, which reinforces the sample immediately. Yet, as temperature drops below 0°C, both ice and unfrozen water still co-exist. Phase change would continue over a range of temperature rather than at a single definite point. This accounts for the gradual increase in E_{11} during the cooling process. The transverse shear modulus of the sample, however, does not exhibit a jump during the freezing process. At low temperatures, it was found that G_{13} shows an approximately linear temperature dependence.

Effectiveness of the dynamic characterization technique can be checked by comparing the present E_{11} and G_{13} results with some published data. It has been found by Dutta and Hui [13] that E_{11} of the original sample (before soaking and drying processes) varies from 27.72 to 28.63 GPa as temperature drops from 24 to −60°C. The results are in agreement with the values quoted in Table 5. Over the same temperature range, however, they reported that G_{13} is bound by 1.10 and 1.31 GPa which is far less than that expected from the present study. The fact that G_{13} should be larger than the shear modulus of pure resin justifies the higher G_{13} value as obtained from the present study. To get a glimpse of the accuracy of the dynamic characterization technique, a numerical sensitivity study is undertaken. Suppose the frequency measurements f_1 and f_2 are erroneous each bearing an error of Δf. Hence, the true frequencies of the sample are bounded by $f_1 \pm \Delta f$ and $f_2 \pm \Delta f$, respectively. The measurement error Δf will eventually get into the inverse calculation scheme and affect the accuracy of the characterized moduli. Consider as an example the original sample at 24°C whose frequency measurements are $f_1 = 1333.0$ Hz and $f_2 = 3173.8$ Hz and the corresponding dynamic moduli are $E_{11} = 25.407$ GPa and $G_{13} = 5.010$ GPa. Since the frequency spectrum has a resolution of 4.88 Hz, each frequency measurement may carry a maximum discretization error Δf of 2.44 Hz. Table 8 presents the characterization results if one regards $f_1 \pm \Delta f$ and $f_2 \pm \Delta f$ as the frequency inputs for the inverse calculation. Recall that the actual frequencies of the sample fall in the ranges $f_1 \pm \Delta f$ and $f_2 \pm \Delta f$, the true values of E_{11} or G_{13} should be bounded by the smallest and largest values in the corresponding table. The maximum percentage deviations of the current values $E_{11} = 25.407$ GPa and $G_{13} = 5.010$ GPa from their exact values are only 0.5 and 2.2%, respectively.

Table 8
Characterized E_{11} and G_{13} values from discrete frequency measurements

	E_{11} (GPa)		G_{13} (GPa)	
	$f_1 - \Delta f$	$f_1 + \Delta f$	$f_1 - \Delta f$	$f_1 + \Delta f$
$f_2 - \Delta f$	25.285	25.568	5.043	4.912
$f_2 + \Delta f$	25.242	25.529	5.121	4.977

Apart from the discretization error, the effects of measurement error on the characterized moduli can be disclosed utilizing Table 8. To proceed, the sensitivities of E_{11} and G_{13} with respect to the individual frequencies are first evaluated. For convenience, the resulting values are put in a sensitivity matrix:

$$\begin{bmatrix} \frac{\partial E_{11}}{\partial f_1} & \frac{\partial E_{11}}{\partial f_2} \\ \frac{\partial G_{13}}{\partial f_1} & \frac{\partial G_{13}}{\partial f_2} \end{bmatrix} \approx \frac{1}{2\times 2.44}\begin{bmatrix} 25.568 - 25.285 & 25.242 - 25.285 \\ 4.912 - 5.043 & 5.121 - 5.043 \end{bmatrix} = \begin{bmatrix} 0.0580 & -0.0088 \\ -0.0268 & 0.0160 \end{bmatrix} (\text{GPa/Hz})$$

Now suppose the frequency measurements f_1 and f_2 are subject to errors Δf_1 and Δf_2 (in Hz), respectively. Using the truncated Taylor series expansion, error bounds (in GPa) associated with the individual moduli owing to erroneous frequency measurements can be estimated using the expressions

$$\Delta E_{11} \approx 0.0580 \times \Delta f_1 + (-0.0088) \times \Delta f_2$$

$$\Delta G_{13} \approx (-0.0268) \times \Delta f_1 + 0.0160 \times \Delta f_2 \quad (7)$$

These expressions indicate that both the longitudinal and transverse shear moduli are insensitive to the measurement errors, especially Δf_2, owing to the small sensitivity values contained in the sensitivity matrix. This, together with the accurate frequency measurement, renders the characterization process very accurate.

8. Conclusions

The present study has examined the flexural vibration response of a thick S2-glass composite beam over a temperature range from −80 to 24°C. Through the development of an inverse calculation scheme, hygrothermal effects on the longitudinal and transverse shear moduli of the constituting material were also revealed. Impact testing is proven to be a reliable and convenient way to extract the vibration characteristics of beams under a severe environmental condition. It was found that both frequency and stiffness of the sample increase with reducing temperature. At the lowest temperature being considered, i.e. −80°C, the dried sample shows a 4.57 and 19.23% gain in its E_{11} and G_{13} values from the room temperature values. Even a small amount of moisture (0.93% of the sample weight) can raise these percentages to 24.93 and 43.55%. Addition of moisture therefore magnifies the sensitivity of each modulus to temperature. Moistures also cause a sudden change in frequency values at 0°C. The abrupt frequency variation is attributed to the severe change in E_{11}. Such property change is more pronounce when the sample has higher moisture content. After all, for the composite material under consideration, G_{13} is susceptible to temperature variation over the entire temperature range whereas E_{11} is sensitive to freezing of moistures.

Acknowledgements

This paper is an extended version of the earlier work 'Influence of Low Temperature and Moisture on The Dynamic Moduli of Thick Composite Beams', by Kim Ho Ip, Piyush K. dutta and David Hui, Proc. SPIE Vol. 2921, pp. 676–681, International Conference on Experimental Mechanics: Advances and Applications, Fook S. Chau, C.T. Lim (eds.) December 1996.

References

[1] Hertz J, Investigation into the high-temperature strength degradation of fiber-reinforced resin composite during ambient aging. General Dynamics/Convair Aerospace Division, Report GDCA-DBG73-005, 1973.

[2] Allred RE. The effect of temperature and moisture content on the flexural response of Kevlar/Epoxy laminates: Part I. [0/90] Filament orientation. In: Springer GS, editor. Environmental effects on composite materials, vol. 2. Lancaster, PA: Technomic Publishing Company, 1984. p. 27–42.

[3] Allred RE. The effect of temperature and moisture content on the flexural response of Kevlar/Epoxy laminates: Part II. [±45,0/90] Filament orientation. In: Springer GS, editor. Environmental effects on composite materials, vol. 2. Lancaster, PA: Technomic Publishing Company, 1984. p. 43–58.

[4] Gibson RF, Yau A, Mende EW, Osborn WE. The influence of environmental conditions on the vibration characteristics of chopped-fiber-reinforced composite materials. In: Springer GS, editor. Environmental effects on composite materials, vol. 2. Lancaster, PA: Technomic Publishing Company, 1984. p. 79–94.

[5] Lee MC, Peppas NA. Water transport in epoxy resins. Prog Polym Sci — Int Rev J 1993;18(5):947–61.

[6] Fischer S, Roman I, Harel H, Marom G, Wagmer HD. Simultaneous determination of shear and young's moduli in composites. J Testing Evaluat 1981;9(5):303–7.

[7] Timoshenko SP. On the correction for shear of the differential equation for transverse vibration of prismatic bars. Phil Mag Ser 6 1921;41:744–6.

[8] Thomson WT. Theory of vibration with applications. 3rd ed. Englewood Cliffs, NJ: Prentice Hall, 1988 p. 221–6, revised printing.

[9] White MWD, Heppler GR. Vibration modes and frequencies of Timoshenko beams with attached rigid bodies. J Appl Mech 1995; 62:193–9.

[10] Huang TC. The effect of rotatory inertia and of shear deformation on the frequency and normal mode equations of uniform beams with simple end conditions. J Appl Mech 1961;28:579–84.

[11] Levinson M, Cooke DW. On the two frequency spectra of Timoshenko beams. J Sound Vibr 1982;84(3):319–26.

[12] Jones RM. Mechanics of composite materials. Washington, DC: Scripta Book Company, 1975–1988. p. 90–1.

[13] Dutta PK, Hui D. Low-temperature and freeze-thaw durability of thick composites. Composites: Part B 1996;27B(3/4):371–9.